

## Nonlinear Electron-Phonon Coupling in Doped Manganites

V. Esposito,<sup>1,\*</sup> M. Fechner,<sup>2,3</sup> R. Mankowsky,<sup>2,4</sup> H. Lemke,<sup>5,6</sup> M. Chollet,<sup>5</sup> J. M. Glowia,<sup>5</sup> M. Nakamura,<sup>7</sup> M. Kawasaki,<sup>7,8</sup> Y. Tokura,<sup>7,8</sup> U. Staub,<sup>1</sup> P. Beaud,<sup>1,6,‡</sup> and M. Först<sup>2,4,†</sup>

<sup>1</sup>Swiss Light Source, Paul Scherrer Institut, 5232 Villigen PSI, Switzerland

<sup>2</sup>Max-Planck Institute for the Structure and Dynamics of Matter, 22761 Hamburg, Germany

<sup>3</sup>Materials Theory, ETH Zürich, Wolfgang-Pauli-Strasse 27, 8093 Zürich, Switzerland

<sup>4</sup>Center for Free Electron Laser Science, 22761 Hamburg, Germany

<sup>5</sup>LCLS, SLAC National Accelerator Laboratory, Menlo Park, California 94025, USA

<sup>6</sup>SwissFEL, Paul Scherrer Institut, 5232 Villigen PSI, Switzerland

<sup>7</sup>RIKEN Center for Emergent Matter Science, Wako 351-0198, Japan

<sup>8</sup>Department of Applied Physics and Quantum Phase Electronics Center (QPEC), University of Tokyo, Tokyo 113-8656, Japan

(Received 20 December 2016; published 15 June 2017)

We employ time-resolved resonant x-ray diffraction to study the melting of charge order and the associated insulator-to-metal transition in the doped manganite  $\text{Pr}_{0.5}\text{Ca}_{0.5}\text{MnO}_3$  after resonant excitation of a high-frequency infrared-active lattice mode. We find that the charge order reduces promptly and highly nonlinearly as function of excitation fluence. Density-functional theory calculations suggest that direct anharmonic coupling between the excited lattice mode and the electronic structure drives these dynamics, highlighting a new avenue of nonlinear phonon control.

DOI: 10.1103/PhysRevLett.118.247601

Some of the most fascinating phenomena in condensed-matter physics arise from electron-phonon interactions. A striking example is the BCS theory for superconductivity, where phonons mediate an attractive interaction between two electrons [1]. In metals and semiconductors, transport properties are also shaped by linear electron-phonon (*e*-ph) coupling, in particular through the creation of polarons [2]. Furthermore, *e*-ph coupling plays an important role in the physics of perovskite oxides such as the mixed-valence manganites, where a variety of electronic and magnetic phases is stabilized via the Jahn-Teller effect [3]. The precarious equilibrium between these possible ground states is easily perturbed by external stimuli such as static electric or magnetic fields, temperature, pressure, or even by light, opening new ways of manipulating matter on ever faster time scales with short laser pulses [4–10].

The recent progress in the generation of high-energy ultrashort pulses in the midinfrared (mid-IR) range permits us to resonantly excite vibrational modes of the lattice to large amplitudes, exceeding several percent of the interatomic distances—a value at which nonlinear coupling of phonons to other degrees of freedom becomes important [11–13]. This approach enabled mode-selective material control on subpicosecond time scales, as exemplified in vibrationally induced superconductivity [8,12] and insulator-metal transitions [11], as well as lattice-driven suppression of magnetic and orbital order [14]. A proposed mechanism, referred to as “nonlinear phononics” and based on nonlinear phonon-phonon coupling, suggests that these phenomena result from the rectification of the excited mode and a net displacement of the crystal lattice along the

coordinates of anharmonically coupled vibrational modes, which control the electronic properties [8,14–16]. A possible direct coupling between the excited mode and the electronic system has only seldomly been considered [17], although, for example, the vibrational excitation of a molecular solid was shown to coherently perturb electronic interactions [18].

In this Letter, we explore the nonlinear electron-phonon coupling in a manganite by investigating the lattice driven ultrafast insulator-metal transition [11]. We use resonant x-ray diffraction at the Mn *K* edge to study the dynamics of the electronic and structural order in a  $\text{Pr}_{0.5}\text{Ca}_{0.5}\text{MnO}_3$  (PCMO) thin film driven by large-amplitude excitation of a vibrational mode with 200-fs mid-IR pulses. We then compare our experimental findings with *ab initio* calculations.

At room temperature,  $\text{Pr}_{0.5}\text{Ca}_{0.5}\text{MnO}_3$  is a paramagnetic semiconductor that undergoes a large distortion of the cubic perovskite structure. Charge and orbital order (COO) and antiferromagnetic phases arise upon cooling below  $T_{CO} = 240$  K and  $T_N = 150$  K, respectively [3]. This so-called CE-type COO is characterized by a zigzag arrangement of the  $3d e_g$  orbitals and a checkerboard pattern of  $\text{Mn}^{3+}/\text{Mn}^{4+}$  ions [Fig. 1(a)]. The long-range ordering of the electrons goes in hand with a structural distortion due to the Jahn-Teller effect at the  $\text{Mn}^{3+}$  sites, which lowers the crystal symmetry from orthorhombic *Pbnm* to monoclinic  $P2_1/m$ , and a doubling of the unit cell along the *b* axis, leading to weak superlattice reflections of the type  $[h(k/2)l]$ .

The 40-nm PCMO thin film was grown by pulsed laser deposition on a (011)-oriented  $(\text{LaAlO}_3)_{0.3}(\text{Sr}_2\text{TaAlO}_6)_{0.7}$

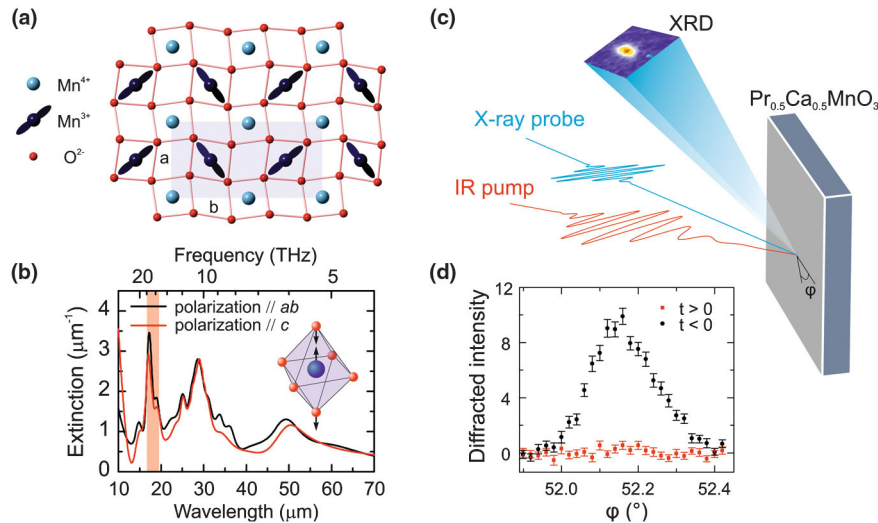


FIG. 1. (a) Charge and orbital order in PCMO in the  $ab$  plane. The low-temperature unit cell is delimited by the blue shaded area. (b) Absorption spectra of a  $\text{Nd}_{0.5}\text{Ca}_{0.5}\text{MnO}_3$  single crystal in the mid-IR range (reproduced from Ref. [19]). This material displays a very similar phase diagram than PCMO and has the same structure and COO pattern below  $T_{CO}$ . The shaded red area represents the spectral range of the pump. The inset shows the dominant motion driven by the excitation. (c) Experimental setup at the XPP beam line at the LCLS. The angle  $\phi$  indicates the rotation angle around the sample's surface normal. (d) Rotational scan around the sample surface normal [angle in panel (c)] of the  $(0\bar{3}0)$  reflection before and 4 ps after excitation at a pump fluence of  $10.7 \text{ mJ}/\text{cm}^2$ . The complete suppression of the Bragg peak after photoexcitation demonstrates the melting of the COO.

substrate, as described in [20], and has an ordering temperature  $T_{CO}$  of 220 K, only slightly below the reported bulk critical temperature. During the experiment, the sample was kept at 100 K, well below  $T_{CO}$ , by means of a nitrogen cryoblower. The sample was excited with 200-fs mid-IR pulses produced by mixing the signal and idler from a high-energy optical parametric amplifier (OPA) seeded by the 800-nm output of an amplified Ti:sapphire laser. The OPA output wavelength was tuned to the stretching mode of the apical Mn-O bond ( $\lambda \approx 17 \mu\text{m}$ , bandwidth  $1.5 \mu\text{m}$ ) with a maximum energy per pulse of  $33 \mu\text{J}$  [Fig. 1(b)]. The subsequent dynamics were probed by resonant x-ray diffraction at the Mn  $K$  edge with monochromatized 50-fs pulses provided by the Linac Coherent Light Source (LCLS) free electron laser at the SLAC National Accelerator Laboratory. To guarantee an optimum time resolution the arrival time difference between the pump and the probe was measured shot to shot by means of the spectral encoding technique [21]. A sketch of the pump-probe experiment that was carried out at the XPP instrument [22] is shown in Fig. 1(c). The probed area is homogeneously excited due to the relatively large  $280 \times 750 \mu\text{m}^2$  pump spot (versus  $50 \times 50 \mu\text{m}^2$  for the x-ray beam).  $P$ -polarized light ensures maximum power transmitted into the sample. Because the penetration depth of the mid-IR (360 nm) is much larger than the film thickness (40 nm), the excitation density can be considered as uniform over the entire probe volume. Optimization of various geometrical constraints leads to the noncollinear

geometry of the experiment [see Fig. 1(c)]; more details can be found in the Supplemental Material [23].

The charge-order (CO) response is measured by the intensity of the  $(0\bar{3}0)$  reflection at the Mn  $K$  edge, which directly relates to the charge disproportionation at the Mn sites [29]. Figure 1(d) shows the disappearance of the  $(0\bar{3}0)$  Bragg peak 200 fs after excitation at a fluence of  $10.7 \text{ mJ}/\text{cm}^2$ , demonstrating complete charge- and orbital-order melting. The dynamics of the charge-order peak for different excitation fluence are shown in Fig. 2(a). Minor intensity changes are observed below  $5 \text{ mJ}/\text{cm}^2$ . Above a critical fluence of  $f_c = 8.7 \text{ mJ}/\text{cm}^2$ , the  $(0\bar{3}0)$  reflection disappears within the experimental time resolution of  $\sim 200$  fs, clearly evidencing prompt CO melting. In a narrow range of intermediate fluences, the CO is only partially melted and recovers over several tens of picoseconds. The fluence dependence of the intensity drop, shown in Fig. 2(b), highlights this nonlinear, thresholdlike behavior. In contrast, above-band gap excitation at near-IR 800-nm wavelengths, which directly perturbs the electronic system, results in prompt charge-order melting with a linear fluence dependence [10], as shown in the overlaid data.

We performed density-functional theory (DFT) calculations to identify the lattice dynamics induced by the intense midinfrared excitation and their effects on the electronic structure. The first-principles calculations are performed in the framework of density functional theory using the generalized gradient approximation [30] as implemented within the Vienna *ab initio* simulation package (VASP) [31].

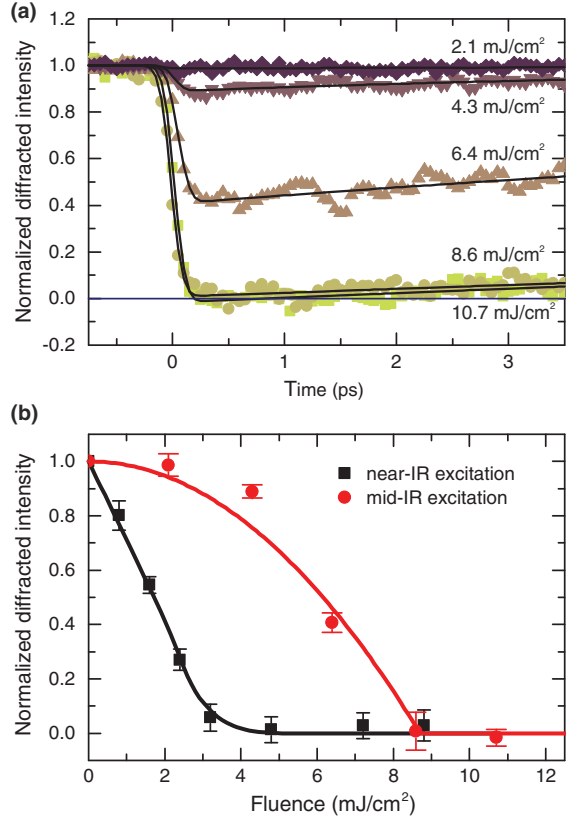


FIG. 2. Dynamic of charge-order melting. (a) Transient response of the  $(0\bar{3}0)$  charge-order reflection for different fluence ( $\lambda = 17 \mu\text{m}$ ). The time traces were taken at the maximum intensity of the Bragg peak [Fig. 1(d)]. The error bars are about 1.5 times the symbol size and are not displayed for clarity. The black lines are fits to the data consisting of an error function with an exponential recovery. (b) Whereas excitation with near-IR pulses leads to a linear drop in diffraction intensity as a function of fluence and can be described by the Landau-type order parameter proposed in Ref. [10] (black squares and line), the intensity drop following mid-IR excitation is highly nonlinear. The red circles are the maximal drop given from the fit of the time-evolution traces and the red line is a fit using  $1 - (f/f_c)^2$ , yielding a critical fluence of  $8.7 \pm 0.7 \text{ mJ/cm}^2$ .

More details on the DFT and phonon calculation are given in the Supplemental Material [23]. The analysis of the zone-center phonon modes reveals that only two infrared-active modes at 17.2 and 18.9 THz are significantly excited by the  $c$  axis polarized mid-IR pulse. The ionic motion of these modes, which besides the main Mn-O stretching sketched in Fig. 1(b) also exhibit small displacements within the  $ab$  plane, are presented in the Supplemental Material [23]. First, we consider the anharmonic coupling of these modes to Raman modes within the framework of nonlinear phononics. As opposed to Ref. [17], however, we use the low-temperature charge-ordered  $P2_1/m$  structure [23]. Mapping the total energies of our DFT calculations onto the full phonon-phonon potential  $V = \omega_{\text{IR}}^2 Q_{\text{IR}}^2 + \omega_R^2 Q_R^2 + a_3 Q_R Q_{\text{IR}}^2 + \dots$ ,

we find that both excited IR modes couple only weakly (as  $a_3/\omega_R^2$ ) to Raman modes, displacing the lattice along the coordinates of low-frequency  $A_g$  modes by a maximum of  $0.05\sqrt{u\text{\AA}}$  [23]. This atomic motion is more than 1 order of magnitude smaller than observed in  $\text{YBa}_2\text{Cu}_3\text{O}_{6.5}$ , where the enhancement of superconductivity was shown to be the consequence of such lattice anharmonicity [8,16]. Furthermore, the PCMO band gap reduction induced by the atomic motions of the nonlinearly coupled  $A_g$  Raman modes scales linearly with the excitation fluence [23], suggesting that the nonlinear phononics mechanism is likely not driving the insulator-metal transition.

Hence, we explore the changes of the electronic structure due to the atomic displacement along the coordinates of the directly excited IR mode. The CO state is stabilized by the creation of an electronic gap ( $E_g$ ), whose lattice-induced alterations are computed within the frozen phonon approximation for both modes. Indeed, we find a quartic reduction of the gap size as a function of both mode amplitudes, which at large values close the band gap as shown in Fig. 3(a).

To confront this finding with the experimental observation, we calculate the fluence-dependent amplitudes of the IR modes by numerically solving the equations of motion [32]. For simplicity, we assume that the electronic gap is determined by the maximum phonon amplitude  $Q_{\text{IR,max}}^4$  of the directly driven phonon modes, which is reached at the end of the mid-IR excitation pulse. However, we cannot rule out that dynamically the gap size reduces with the time average  $\langle Q_{\text{IR}}^4 \rangle$  of these modes. Figure 3(b) shows the calculated gap size for both individually excited modes and their summed contribution, revealing a critical pump fluence of  $f_c = 5.4 \text{ mJ/cm}^2$  for a full gap closure. This value is slightly lower than the experimental value of  $8.7 \text{ mJ/cm}^2$ . However, when taking into account the  $32^\circ$  angle between the mid-IR pump electric field and the  $c$  axis, the estimated experimental critical fluence reduces by 28% to  $f_c \approx 6.3 \text{ mJ/cm}^2$ , which is in excellent agreement with the calculation. As both the calculated gap energy and the measured  $(0\bar{3}0)$  Bragg intensity represent the square of the charge-order parameter [33], these quantities can be directly compared. A quadratic function fit, as expected from the square reduction of the gap energy with excitation fluence, reproduces the measured diffracted intensity drop reasonably well [see Fig. 2(b)].

We further probed the dynamics of the crystal lattice by measuring two superlattice reflections (Fig. 4): the  $(0\bar{2}\bar{2}0)$  peak, sensitive to the Jahn-Teller distortion and orbital order at the  $\text{Mn}^{3+}$  sites, and the  $(\bar{2}\bar{2}\bar{2}0)$  peak, a direct measure of the overall structural distortion that accompanies the charge and orbital ordering. The fast drop in diffracted intensity and the coherent 2.4-THz modulations for both reflections indicate a displacive excitation of atomic motions towards the high-symmetry phase triggered by the melting of the COO

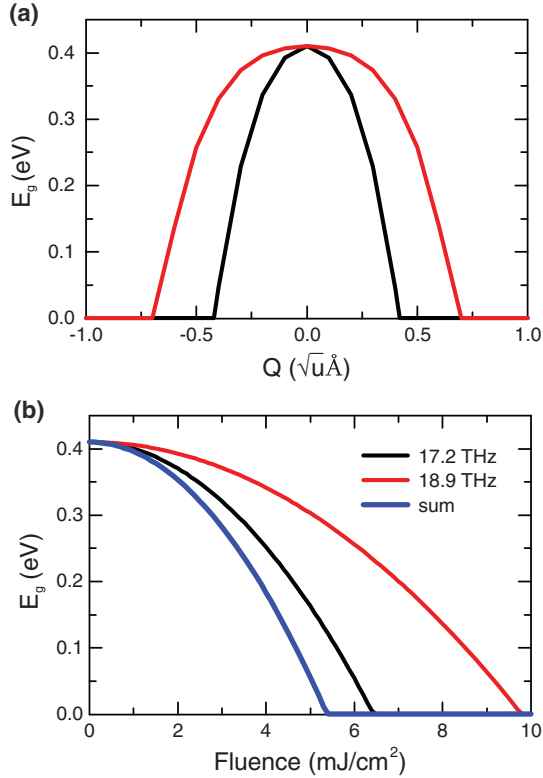


FIG. 3. (a) Calculated gap energy as a function of the frozen amplitude of the two excited IR modes. Interestingly, the quadratic coefficient also vanishes and the coupling is found to be purely quartic. The phonon amplitude  $Q$  is given in units of  $\sqrt{u}\text{\AA}$ , where  $u$  is the atomic mass. (b) The electronic gap as a function of mid-IR fluence for the two excited IR modes and their summed contribution. All other contributions, from additional IR modes or coupled Raman phonons, are found to be negligible (see Supplemental Material [23]).

[10,34]. The same relaxation and coherent dynamics were observed earlier, when prompt melting of the charge order was induced by direct excitation of the electronic system [10]. The similarities suggest that the structural dynamics are initiated by CO melting in both cases.

The phenomenological model, describing charge-order dynamics induced by exciting the electronic system in the near-IR, proposes the charge-order parameter  $\eta = \sqrt{1 - n/n_c}$  in the driven state to depend solely on the excess energy in the electronic system [10]. A critical excitation density of  $500 \text{ J/cm}^3$  was required for the phase transition to occur. Assuming linear extinction, the direct lattice excitation investigated here requires a significantly lower critical excitation density of  $200 \text{ J/cm}^3$ .

Once the electronic gap becomes smaller than the mid-infrared photon energy, direct photo doping into the electronic system sets in, possibly leading to nonlinear absorption. The details of these dynamics could be experimentally investigated by monitoring the CO during the pump pulse, an experiment that requires carrier-envelope

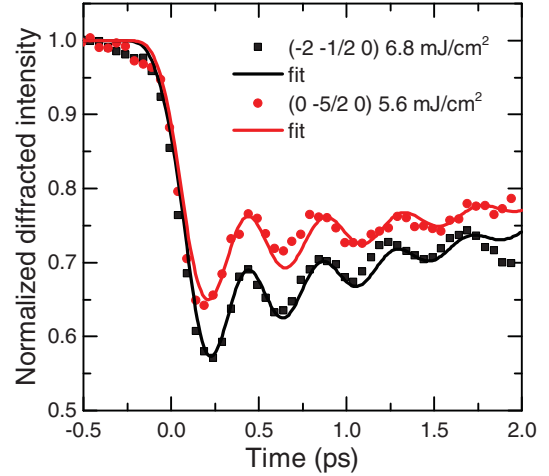


FIG. 4. Response of the structural superlattice reflection  $(\bar{2}\frac{3}{2}0)$  and the orbital order reflection  $(0\bar{5}\frac{5}{2}0)$  at intermediate pump fluence. As for excitation of the electronic system at near-IR wavelength, a 2.4-THz coherent oscillation around a new equilibrium position is observed, suggesting a displacive excitation mechanism triggered by the fast melting of charge and orbital order in both cases. The solid lines are fits of an exponential recovery and a damped oscillation.

phase-stable mid-IR pulses and a high time resolution. Further insight on the energy balance between the lattice and the electrons will be gained once time-resolved dynamical calculations become feasible for such large systems. In addition, a comprehensive characterization of the photo-induced transient state is still missing and other crucial aspects of the transition need to be explored. The spin dynamics and the magnetic ordering have been completely ignored here [35], yet in the manganites transport properties are tightly bound to the magnetic state.

In summary, we have shown that the melting of the charge and orbital order following coherent lattice excitation in PCMO are driven by the direct and highly nonlinear coupling between the excited IR modes and the electronic degrees of freedom. As the gap closes, the charge and orbital order is suppressed and the Jahn-Teller distortion released, triggering structural relaxation. When combined with DFT calculations, the observed nonlinear behavior is well explained by the quartic dependence of the electronic gap on the excited phonon amplitude. This is an example of a new and direct way of phonon control of materials, where the electron-phonon interaction is pushed to the nonlinear regime, allowing coupling with odd-parity modes.

This work was supported by the National Centres of Competence in Research (NCCR) Molecular Ultrafast Science and Technology (NCCR Molecular Ultrafast Science and Technology), a research instrument of the Swiss National Science Foundation (SNSF). Use of the Linac Coherent Light Source (LCLS), SLAC National Accelerator Laboratory, is supported by the U.S.

Department of Energy, Office of Science, Office of Basic Energy Sciences under Contract No. DE-AC02-76SF00515. M.N. was supported by the Japan Science and Technology Agency (JST), Precursory Research for Embryonic Science and Technology (PRESTO).

\*vincent.esposito@psi.ch

†michael.foerst@mpsd.mpg.de

\*paul.beaud@psi.ch

- [1] J. Bardeen, L. N. Cooper, and J. R. Schrieffer, *Phys. Rev.* **108**, 1175 (1957).
- [2] G. D. Mahan, *Many-Particle Physics*, 3rd ed. (Springer Science & Business Media, New York, 2000).
- [3] E. Dagotto, *Nanoscale Phase Separation and Colossal Magnetoresistance: The Physics of Manganites and Related Compounds* (Springer, New York, 2003).
- [4] K. Miyano, T. Tanaka, Y. Tomioka, and Y. Tokura, *Phys. Rev. Lett.* **78**, 4257 (1997).
- [5] F. Schmitt, P. S. Kirchmann, U. Bovensiepen, R. G. Moore, L. Rettig, M. Krenz, J.-H. Chu, N. Ru, L. Perfetti, D. Lu *et al.*, *Science* **321**, 1649 (2008).
- [6] T. Kampfrath, A. Sell, G. Klatt, A. Pashkin, S. Mährlein, T. Dekorsy, M. Wolf, M. Fiebig, A. Leitenstorfer, and R. Huber, *Nat. Photonics* **5**, 31 (2011).
- [7] G. Coslovich, B. Huber, W.-S. Lee, Y.-D. Chuang, Y. Zhu, T. Sasagawa, Z. Hussain, H. Bechtel, M. Martin, Z.-X. Shen *et al.*, *Nat. Commun.* **4**, 2643 (2013).
- [8] R. Mankowsky, A. Subedi, M. Först, S. Mariager, M. Chollet, H. Lemke, J. Robinson, J. Glownia, M. Minitti, A. Frano *et al.*, *Nature (London)* **516**, 71 (2014).
- [9] T. Kubačka *et al.*, *Science* **343**, 1333 (2014).
- [10] P. Beaud, A. Caviezel, S. Mariager, L. Rettig, G. Ingold, C. Dornes, S. Huang, J. Johnson, M. Radovic, T. Huber *et al.*, *Nat. Mater.* **13**, 923 (2014).
- [11] M. Rini, R. Tobey, N. Dean, J. Itatani, Y. Tomioka, Y. Tokura, R. W. Schoenlein, and A. Cavalleri, *Nature (London)* **449**, 72 (2007).
- [12] D. Fausti, R. Tobey, N. Dean, S. Kaiser, A. Dienst, M. C. Hoffmann, S. Pyon, T. Takayama, H. Takagi, and A. Cavalleri, *Science* **331**, 189 (2011).
- [13] M. Först, C. Manzoni, S. Kaiser, Y. Tomioka, Y. Tokura, R. Merlin, and A. Cavalleri, *Nat. Phys.* **7**, 854 (2011).
- [14] M. Först, R. I. Tobey, S. Wall, H. Bromberger, V. Khanna, A. L. Cavalieri, Y.-D. Chuang, W. S. Lee, R. Moore, W. F. Schlotter, J. J. Turner, O. Krupin, M. Trigo, H. Zheng, J. F. Mitchell, S. S. Dhesi, J. P. Hill, and A. Cavalleri, *Phys. Rev. B* **84**, 241104 (2011).
- [15] A. Subedi, A. Cavalleri, and A. Georges, *Phys. Rev. B* **89**, 220301 (2014).
- [16] M. Fechner and N. A. Spaldin, *Phys. Rev. B* **94**, 134307 (2016).
- [17] M. Kim, Y. Nomura, M. Ferrero, P. Seth, O. Parcollet, and A. Georges, *Phys. Rev. B* **94**, 155152 (2016).
- [18] R. Singla, G. Cotugno, S. Kaiser, M. Först, M. Mitrano, H. Y. Liu, A. Cartella, C. Manzoni, H. Okamoto, T. Hasegawa, S. R. Clark, D. Jaksch, and A. Cavalleri, *Phys. Rev. Lett.* **115**, 187401 (2015).
- [19] K. Tobe, T. Kimura, and Y. Tokura, *Phys. Rev. B* **69**, 014407 (2004).
- [20] D. Okuyama, M. Nakamura, Y. Wakabayashi, H. Itoh, R. Kumai, H. Yamada, Y. Taguchi, T. Arima, M. Kawasaki, and Y. Tokura, *Appl. Phys. Lett.* **95**, 152502 (2009).
- [21] M. Harmand, R. Coffee, M. Bionta, M. Chollet, D. French, D. Zhu, D. Fritz, H. Lemke, N. Medvedev, B. Ziaja *et al.*, *Nat. Photonics* **7**, 215 (2013).
- [22] M. Chollet, R. Alonso-Mori, M. Cammarata, D. Damiani, J. Defever, J. T. Delor, Y. Feng, J. M. Glownia, J. B. Langton, S. Nelson, K. Ramsey, A. Robert, M. Sikorski, S. Song, D. Stefanescu, V. Srinivasan, D. Zhu, H. T. Lemke, and D. M. Fritz, *J. Synchrotron Radiat.* **22**, 503 (2015).
- [23] See Supplemental Material at <http://link.aps.org/supplemental/10.1103/PhysRevLett.118.247601> for additional information on the experimental geometry and the *ab initio* phonon calculation, which includes Refs. [24–28].
- [24] R. J. Goff and J. P. Attfield, *Phys. Rev. B* **70**, 140404 (2004).
- [25] A. Togo and I. Tanaka, *Scr. Mater.* **108**, 1 (2015).
- [26] P. E. Blöchl, *Phys. Rev. B* **50**, 17953 (1994).
- [27] V. I. Anisimov, F. Aryasetiawan, and A. Lichtenstein, *J. Phys. Condens. Matter* **9**, 767 (1997).
- [28] Y. Okimoto, Y. Tomioka, Y. Onose, Y. Otsuka, and Y. Tokura, *Phys. Rev. B* **59**, 7401 (1999).
- [29] M. v. Zimmermann, J. P. Hill, D. Gibbs, M. Blume, D. Casa, B. Keimer, Y. Murakami, Y. Tomioka, and Y. Tokura, *Phys. Rev. Lett.* **83**, 4872 (1999).
- [30] J. P. Perdew, K. Burke, and M. Ernzerhof, *Phys. Rev. Lett.* **77**, 3865 (1996).
- [31] G. Kresse and J. Furthmüller, *Phys. Rev. B* **54**, 11169 (1996).
- [32] D. M. Juraschek, M. Fechner, and N. A. Spaldin, *Phys. Rev. Lett.* **118**, 054101 (2017).
- [33] K. A. Ross, Y. Qiu, J. R. D. Copley, H. A. Dabkowska, and B. D. Gaulin, *Phys. Rev. Lett.* **112**, 057201 (2014).
- [34] A. Caviezel, S. O. Mariager, S. L. Johnson, E. Möhr-Vorobeva, S. W. Huang, G. Ingold, U. Staub, C. J. Milne, S.-W. Cheong, and P. Beaud, *Phys. Rev. B* **87**, 205104 (2013).
- [35] T. Li, A. Patz, L. Mouchliadis, J. Yan, T. A. Lograsso, I. E. Perakis, and J. Wang, *Nature (London)* **496**, 69 (2013).